J Mater Sci: Mater Med (2011) 22:2823–2832
DOI 10.1007/s10856-011-4461-x

High speed insertion of bone fracture fixation pins: a finite element penetration model with experimental comparisons

Matthew P. Prygoski · Timotius Pasang · Steven R. Schmid · Antony J. Lozier

Received: 21 March 2011 / Accepted: 11 October 2011 / Published online: 1 November 2011

Abstract A new method of bone fracture fixation is considered in which small pins/darts are dynamically inserted into bone to prevent translation and rotation at the fracture site. An ABAQUS model was developed to analyze dart penetration in cortical and cancellous bone for varying dart diameter, material, and velocity, and cortical thickness. The method is advocated for bioresorbable darts, so polylactide (PLA) and magnesium are the materials examined in this study. Numerical results showed that magnesium darts can achieve full penetration in bone while suffering little damage. The PLA darts penetrated thin bone well, but substantial deformation was seen as the cortical thickness increased, especially for small diameter darts. As partial validation, prototype PLA fixation darts were fired into cadaveric bone with a custom nailer. As in the model, the PLA darts could penetrate thin cortices but saw gross deformation when impacted against thicker bone.

1 Introduction

Large bone fractures often require implants in the form of wires, pins, screws and/or bone plates that immobilize the fractured bone and allow healing to occur [1–5]. Shortcomings with these traditional approaches include occasional poor clinical outcomes, the possible requirement to remove the plates or pins in subsequent surgery, as well as invasive surgical procedures needed for implantation. For example, bone plates often require dissection of muscle or removal of tissue from the bone to achieve proper purchase. Such soft tissue trauma is especially painful and requires significant time for proper healing. A new method of bone fracture fixation (Fig. 1) has been proposed in which multiple small fixation darts are inserted into bone with a device similar to a pneumatic or electric nail gun, possibly in an arthroscopic manner [1]. In the proposed method, darts would be driven through the fragments and into substrate bone at high velocity without the use of a pilot hole. During high velocity insertion, inertial forces would keep fragments from translating. The insertion of multiple darts at varying angles can effectively lock a bone fragment in place and facilitate healing [1, 3]. The technology may lend itself well to the insertion of small bioresorbable darts, which are beneficial because they reduce problems associated with stress shielding and eliminate the need for removal surgery [1, 4, 6, 7].

Polylactide (PLA) and magnesium are two materials that would be well-suited for fracture fixation darts. PLA is a relatively strong polymer and has been used extensively for biomedical applications such as bone plates, bone pins and screws, and scaffold materials. Its strength and degradation resistance can be enhanced by increasing its molecular weight and crystallinity. It has been shown to be biocompatible, biodegradable, and bioresorbable [8, 9]. High strength PLA used for implants degrades rather slowly in the body. For example, PLA rods 2 mm in diameter and 35 mm in length were submerged in physiological saline and did not completely lose their bending strength until 18 months had passed [10]. The slow degradation of PLA

M. P. Prygoski · S. R. Schmid (✉)
Department of Aerospace and Mechanical Engineering, University of Notre Dame, 150 Multidisciplinary Research Building, Notre Dame, IN 46637, USA
e-mail: schmid.2@nd.edu

T. Pasang
Department of Mechanical and Manufacturing Engineering, AUT University, Auckland, New Zealand

A. J. Lozier
Zimmer Inc., Warsaw, Indiana, USA

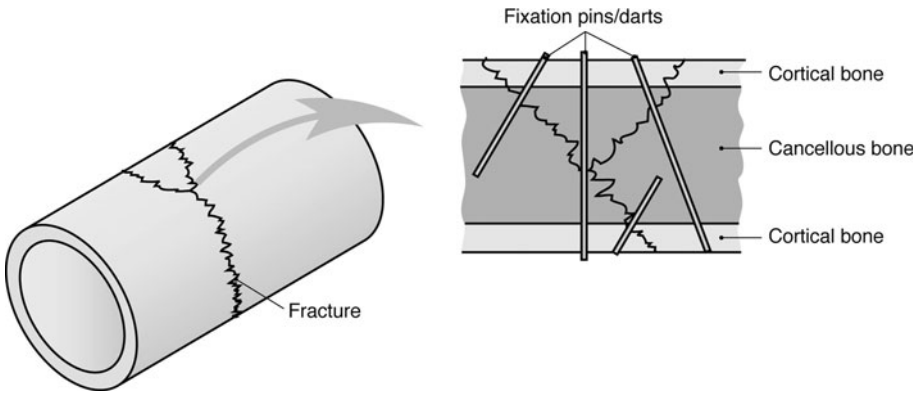

Fig. 1 Schematic illustration of complex fracture, as in the femur. The proposed surgical technique is the use of multiple fixation pins/darts driven across the fracture site to achieve adequate fixation [1]

may also prevent a potentially toxic environment from developing around the implant, as the body can gradually process the lactic acid released during degradation. High acidity has been identified as a potential cause of sterile sinuses around implants made of rapidly degrading polymers such as self-reinforced polyglycolide [10]. As such, the concentration of lactic acid should be considered, especially since multiple PLA pins inserted in close proximity could overwhelm the body's ability to process the byproducts.

Magnesium and its alloys are an attractive implant material because their static mechanical properties are similar to bone and this can reduce the detrimental effects of stress shielding [6, 11–13]. The superior mechanical properties (compared to other resorbables) of magnesium might make it a good candidate for fracture fixation involving large gaps, such as those encountered in multiple fracture or battlefield injuries. Magnesium and its alloys show significant levels of strain hardening and strain rate hardening which would facilitate penetration in hard cortical bone [14]. Biological responses to several magnesium alloys have been explored in small animal studies and the results demonstrate the suitability of magnesium for in vivo applications [15–17]. The degradation products from magnesium may actually stimulate bone growth [6, 13, 15, 16]. Magnesium degrades much more rapidly than PLA in vivo, and the degradation time may be a critical design factor. For example, a 1 g magnesium alloy screw was found to completely degrade in 17 weeks [6]. Similarly, magnesium alloy rods (1.5 mm diameter and 20 mm in length) were found to completely degrade after 18 weeks of implantation in guinea pig femurs [6, 17].

It is expected that there exists a relationship between a dart's size and the thickness of cortical bone the dart is able to penetrate. Typical bone fixation devices such as wires, pins, and screws have a wide range of diameters. Kirschner wires used in the reduction of wrist fractures can be as small as 1.4 mm in diameter [3]. PLA fixation pins of 3.5 mm in diameter have been ultrasonically welded to bone substrates for better fixation [18]. Common bone screws are available in diameters of 2.7, 3.5, and 4.5 mm [19]. Cortical bone thickness varies significantly depending on the individual, age, and anatomical location. Although the femoral cortical bone can be as thin as 2 mm during childhood, it can thicken to between 8–10 mm in some locations by adulthood [20]. Direct measurements of cortical thickness from one femur showed that thickness ranged from 2.4 to 11.2 mm depending on location [21]. The thickness of one radius cortical shell was measured between 2.0 and 4.93 mm as part of a validation for an ultrasonic method [22]. Typical thickness values for the radius have been reported to be between 2.5–3.5 mm and have been found to decrease with age [20]. Micro-CT scans have shown radius cortical shells can be as thin as 0.7 mm [23].

In the present work, a finite element model is developed and employed to assess how dart diameter, cortical shell thickness, and other parameters change the penetration performance of both PLA and magnesium darts. The model will be used to determine which design factors are most influential, as well as to make specific predictions about the success of inserting small diameter PLA darts. Experiments using cadaveric bone will be performed to assess the feasibility of inserting PLA darts at high velocity and to potentially validate a subset of the model results.

2 Methods

2.1 Finite element model

2.1.1 Geometry and convergence

A finite element model was constructed using the ABAQUS/CAE software package [24]. The model consisted of four parts including the dart, needle, nozzle, and bone which included a cortical shell atop a cancellous substrate (Fig. 2). The thin cylindrical nozzle was modeled to radially constrain the dart as an accompanying, relatively massive, needle drove the dart into bone. The geometry of

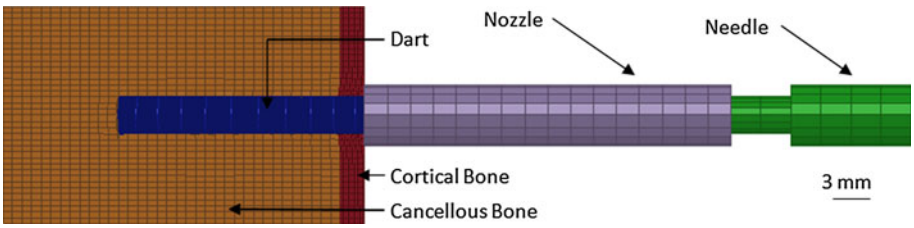

Fig. 2 Cross-sectional view of the FEA model midway through penetration

the needle and nozzle acted to ensure separation of the needle and dart as the leading end of the needle became flush with the bone surface. The dimensions of the bone were scaled with the dart diameter to minimize boundary condition effects and to allow for full penetration of the dart. The sides of the bone substrate were rigidly fixed to simulate attachment to surrounding bone. The nozzle was not allowed to translate.

Each part was modeled with 8-node linear brick reduced integration continuum elements (C3D8R) from the ABAQUS library [24]. Figure 3 illustrates the dependence of different energy terms on number of elements used in the model. This mesh refinement study was performed for the full dynamic analysis, at high speed and with full penetration. Adequate convergence was achieved with 71,000 elements. Over 62,000 of those elements were assigned to the bone with the highest element density in the influential cortical shell. Each simulation required about 8–12 h of computer time using 71,000 elements. ABAQUS/Explicit was used solve the model.

2.1.2 *Material modeling*

Material constitutive models were developed from published data for PLA, magnesium, and cortical and cancellous bone. A high level summary is provided below while a few specific high strain rate values can be found in Table 1.

The dart materials were assumed to be Hookean. Strain rate dependent yield properties were assigned using a von Mises plasticity model. Since strain-rate dependent plastic properties were unavailable for pure PLA, data for a blend of PLA and 5% tri-calcium phosphate (TCP) were used [7]. Data was extrapolated, and ensure that the extrapolated rate-hardening behavior was realistic for a polymer, it was compared to data for both polycarbonate and polymethyl methacrylate [25]. Similarly, strain rate dependent yield behavior was not available for pure magnesium. Instead, data for an alloy of magnesium with 2% aluminum and trace amounts of manganese was used. The magnesium alloy samples showed significant strain hardening and strain rate hardening [14]. The static compressive yield strengths for this alloy were consistent with the wide range of compressive yield strengths (65–100 MPa) for magnesium and its biomedical alloys [6]. The constitutive behaviors of magnesium and PLA are illustrated in Fig. 4.

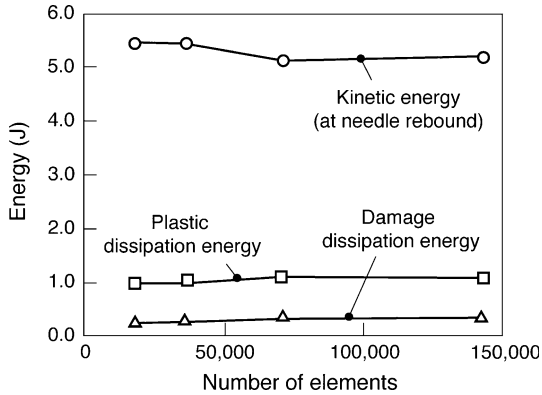

Fig. 3 Different energy related outputs from ABAQUS showed negligible differences between 71,000 and 142,000 elements

Specification of a yield point and an ultimate point allowed for the approximation of strain hardening behavior. Note that ABAQUS only interpolates inside a provided range and does not provide extrapolation of tabulated data [24].

The cortical and cancellous portions of the bone were Hookean in the elastic range. Bone had a similar constitutive model as the PLA and magnesium in the plastic range (Fig. 5). Two constitutive models (Bone 1 and 2) were developed for cortical bone to account for discrepancies in yield and post-yield data. Bone 1 data was taken primarily from the research of Hansen et al. (2008) [26] and displays strain rate softening. The second model, Bone 2 primarily relies on the work of McElhaney et al. (1965) [27] and displays strain rate hardening. The apparent density of cancellous bone was chosen to be 600 kg/m^3 to be consistent with previous work [28–32]. Since strain rate effects were thought to be important, the strain rate dependent ultimate strength data from Linde et al. (1991) [28] was adopted (using the chosen density in fitting functions) as the yield criteria for the current study (Fig. 5). No further extrapolation of this data was undertaken since the validity of the fitting function could not be verified outside of this range.

ABAQUS's damage initiation and evolution material model was used to remove bone elements from the discretization based on a material failure criterion. The onset of damage is controlled by the equivalent plastic strain at failure [24]. The damage initiation parameter was estimated by the difference between the ultimate and yield

Table 1 A summary of the model material properties at the highest available strain rate for PLA, magnesium, cortical bone (both Bone 1 and 2 constitutive models), and cancellous bone

	PLA	Magnesium	Cortical bone 1	Cortical bone 2	Cancellous bone
Density (kg/m^3)	1290 [8]	1,740 [6]	2,100 [19]	2100 [19]	600 [28–32]
Poisson's ratio	0.44 [7]	0.35 [48]	0.37 [49]	0.37 [49]	0.3 (estimated)
Elastic modulus (GPa)	3.7 [7]	41.0 [6]	17 [26]	17 [26]	0.739 [28]
Yield strength (MPa)	132 @ 1,700/s (extrapolated) [7]	101.7 @ 1,659/s [14]	62 @ 17.5/s [26]	284 @ 1,500/s [27]	20.47 @ 10/s [28]
Ultimate strength (MPa)	202 @ 1,700/s (extrapolated) [7]	469 @ 1,659/s [14]	194 @ 17.5/s [26]	323 @ 1,500/s [27]	Ultimate values adopted as yield values
Equivalent yield strain (%)	3.1 @ 1,700/s (extrapolated) [7]	0.25 @ 1,659/s [14]	0.36 @ 17.5/s [26]	1.7 @ 1,500/s [27]	2.8 @ 10/s [28]
Equivalent ultimate strain (%)	7.9 @ 1,700/s (extrapolated) [7]	17 @ 1,659/s [14]	4.2 @ 17.5/s [26]	1.9 @ 1,500/s [27]	Ultimate values adopted as yield values
Equivalent failure strain (%)	N/A	N/A	4.2 @ 17.5/s [26, 33]	1.9 @ 1,500/s [27]	5.0 @ 10/s [28, 35, 36]
Fracture energy (J/m^2)	N/A	N/A	6,716 [38]	6716 [38]	103 [38, 40, 41]

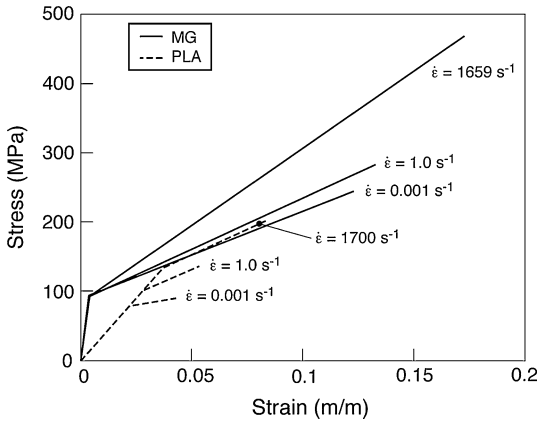

Fig. 4 Constitutive models for both magnesium and PLA showing the approximated strain hardening and strain rate hardening behavior for select strain rates [6, 7, 14]

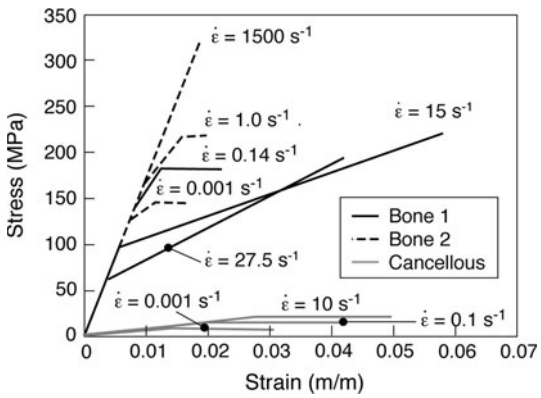

Fig. 5 The constitutive models for cortical and cancellous bone shown at select strain rates. Cortical bone was modeled with a strain rate softening (*Bone 1*) or strain rate hardening (*Bone 2*) behavior [26–28, 33, 35, 36]

strains. For cortical bone, compression and shear induced equivalent strains were considered [26, 33, 34]. For cancellous bone, shear induced equivalent failure strains were adopted since they are typically higher than compressive values [34–37].

Once damage initiates, ABAQUS uses an algorithm to degrade the stiffness, E, and stress carrying capacity, σ, of an element from its nominal value according to the following relationships:

$$E = (1 - d)\bar{E} \tag{1}$$

$$\sigma = (1 - d)\bar{\sigma} \tag{2}$$

here, d, is the damage parameter. The rate of degradation, governed by $\dot{d}$, can be determined in part by the fracture energy of the material. Once the stiffness is negligible, the element is removed from the discretization. The mass is assigned to the nodes which are free to interact with other element surfaces as point masses [24]. The fracture energy of cortical bone was estimated from data concerning the Mode II critical strain energy release rate of older bone [38]. The average plus one standard deviation was adopted to make the data more applicable to younger and healthier bone which requires more energy to fracture [38]. Shear (Mode II) fracture is relevant for dart penetration and also provides an upper bound (compared to tensile fracture) for the critical strain energy release rate in cortical bone [39]. The fracture energy of cancellous bone was unavailable; instead the critical strain energy release rate G was estimated from the fracture toughness K, according to the following relationship where E is the elastic modulus and υ is the Poisson's ratio [40, 41].

$$K^2 = \frac{GE}{1 - \upsilon^2} \tag{3}$$

2.1.3 Parametric studies

The first parametric study examined the effect of dart diameter, cortical thickness, dart material, and cortical bone constitutive model. To model current practices, dart diameters of 1.5, 3.0, and 4.5 mm were considered [3, 18, 19]. Cortical wall thickness was set at 1.0, 2.0, or 4.0 mm which is typical of smaller bones like the radius [22, 23]. Both PLA and magnesium darts were simulated and both cortical bone constitutive models were employed. All combinations of these four parameters were simulated. The initial velocity of the needle was 15 m/s with an initial kinetic energy of 7.2 J which is typical of a pneumatic power source.

The second parametric study focused on insertion speed. The initial velocity of the needle was varied between 5–15 m/s. There was a natural increase in initial kinetic energy as a consequence of the fixed needle mass. The inputs for this study are analogous to changing the power setting on the pneumatic or electric gun.

2.2 Fabrication of PLA darts

Experimental penetration studies were planned for the two-fold purpose of assessing feasibility of the technology and validating the numerical model. A custom pneumatic nailer was designed for insertion of fixation pins. Investigations focused on 1.5 mm diameter PLA darts, which were expected to have marginal penetration performance based on their size and lower strength relative to magnesium [7, 14].

The PLA darts were produced from PLA pellets (PURAC Biomaterials PuraSorb PL 1820 and Boehringer Ingelheim Resomer L 214 Poly (L-lactid)). A capillary rheometer was used to melt PLA pellets inside its heated chamber and inject the molten material into a custom made heated die with a cylindrical cavity (1.5 mm in diameter and 15 cm in length). Different molecular weights and viscosities of the two commercial blends caused the materials to behave slightly differently under similar processing conditions. The PLA came vacuum packed and frozen in pellet form. 10 ml of material was dried in for at least 3 h before molding to avoid moisture related defects upon injection [8, 42]. The chamber melt time, melt temperature, die preheat temperature, and injection rate were all varied in an attempt to produce long rods with minimal defects such as pores and surface pits [8, 42, 43]. Melt temperatures varied between 220–250°C, melt times between 3–6 min, average die temperatures between 140–260°C, and injection ram rates between 100–600 mm/min. Darts of the desired length (2.54 cm) were cut from the defect free sections of the molded rods.

2.3 Cadaveric bone insertion

Insertion trials were performed on a cadaveric humerus, harvested from an elderly donor. A series of the PLA darts was successfully fired into the distal humeral epiphysis after the soft tissue was dissected from the elbow region. Darts were then fired in a path from the distal epiphysis to the shaft of the bone to assess where penetration would become impossible (due to increasing cortical thickness). To ensure the darts achieved full penetration without fracture or deformation, and to assess the thickness of the cortical wall, the bone was sectioned with a surgical saw.

3 Results

3.1 Finite element modeling

The levels of tip deformation were categorized based on a qualitative comparison of the visual results (Fig. 6). Group A saw complete penetration with very low levels of dart tip deformation. Similarly Group B saw very low tip deformation, but only partial penetration, due to the initial kinetic energy being completely consumed through deformation of the bone. Group C saw full penetration, but higher levels of tip deformation that might compromise effective fixation due to excessive clearance between the bone and dart (Fig. 6). Group D had high levels of tip deformation, with either full or incomplete penetration. The results of all 18 simulations have been summarized in Table 2.

Figures 7, 8 show the velocity as a function of penetration depth for particular combinations of dart diameter and cortical bone thickness when using the Bone 1 constitutive model. These figures plot the velocity of the needle since the needle and dart remain in contact throughout the penetration event. The dart does not penetrate a significant amount after separation from the needle due to its low mass and momentum. Results from Group D are not plotted since the very high levels of deformation clearly affected the penetration performance.

Representative results for the second parametric study (varying initial velocity) are shown in Fig. 9 for a 1.5 mm magnesium dart penetrating a 2.0 mm cortical bone (Bone 1) layer. As can be seen the lowest velocities fail to fully penetrate the bone. This model predicts that velocities around 7.5 m/s or higher result in full penetration for these particular parameters.

3.2 Cadaveric bone insertion

When inserted at the distal humeral epiphysis, all darts achieved full penetration and embedded flush with the bone

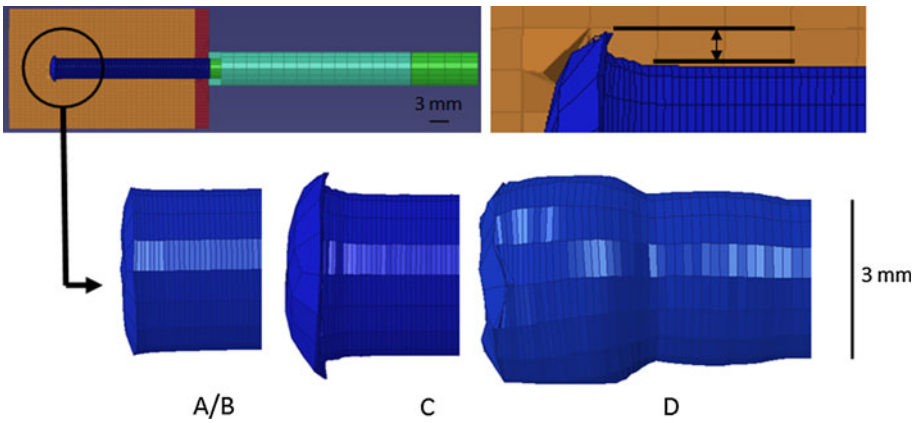

Fig. 6 Typical levels of tip deformation seen in Group *A/B*, Group *C*, and Group *D* (*bottom*). The deformation seen in Groups *C* and *D* might result in a clearance leading to ineffective fixation (*top right*)

Table 2 Summary of results for different combinations of dart material, diameter, and cortical thickness

		Dart diameter		
Bone 1 constitutive model				
Magnesium				
Cortical thickness		1.5 mm	3.0 mm	4.5 mm
	1.0 mm	A	A	B
	2.0 mm	A	A	B
	4.0 mm	A	A	B
PLA				
Cortical thickness		1.5 mm	3.0 mm	4.5 mm
	1.0 mm	C	A	B
	2.0 mm	D	C	B
	4.0 mm	D	D	B
Bone 2 constitutive model				
Magnesium				
Cortical thickness		1.5 mm	3.0 mm	4.5 mm
	1.0 mm	A	A	B
	2.0 mm	A	A	B
	4.0 mm	D	A	B
PLA				
Cortical thickness		1.5 mm	3.0 mm	4.5 mm
	1.0 mm	D	A	B
	2.0 mm	D	C	B
	4.0 mm	D	D	B

A Slight tip deformation, complete penetration, *B* slight tip deformation, incomplete penetration, *C* significant tip deformation, full penetration, *D* gross tip deformation. See Fig. 6 for examples

surface (Fig. 10). Upon sectioning, the bone was estimated to be 1 mm thick or less in this location. Two of the darts were exposed in the cross section, and the tips of other darts could be seen protruding from the second cortical wall (Fig. 11). As the shots progressed towards the humeral shaft, the darts began to fail only a few centimeters away from the successful shots shown in Figs. 10, 11. It was apparent that the cortical thickness increased significantly

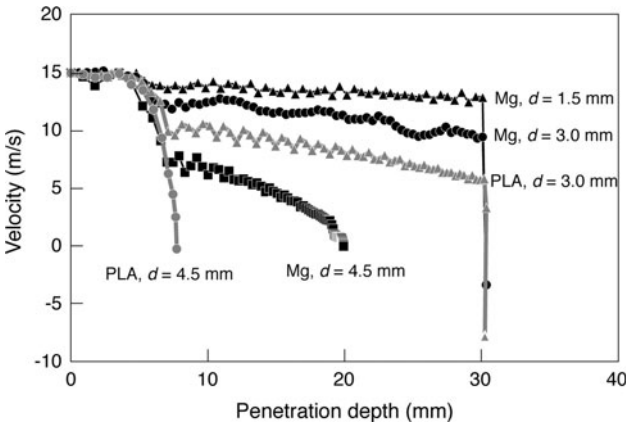

Fig. 7 The effect of dart diameter is examined by holding the cortical bone thickness at a constant 2.0 mm. The Bone 1 constitutive model was used

(2–3 mm) in this transitional region. When fired into the bone mid-shaft, the darts jammed inside the nozzle of the gun. Highly deformed and mushroomed tips effectively eliminated penetration (Fig. 12).

4 Discussion

4.1 Finite element modeling

The results of the model indicate that both magnesium and PLA have potential utility as high-speed fracture fixation darts. According to the model, increasing the dart diameter should more than compensate for cortical bone that might be normally too thick for successful penetration. Incomplete penetration with minor tip deformation occurred with the largest diameter (4.5 mm) but this shortcoming could be overcome with a slightly higher velocity and/or kinetic energy. Dart tip mushrooming could be detrimental for fixation since the deformed tip could plow through the cancellous structure creating clearance between the bone and the dart shaft. Based on this criterion, the magnesium

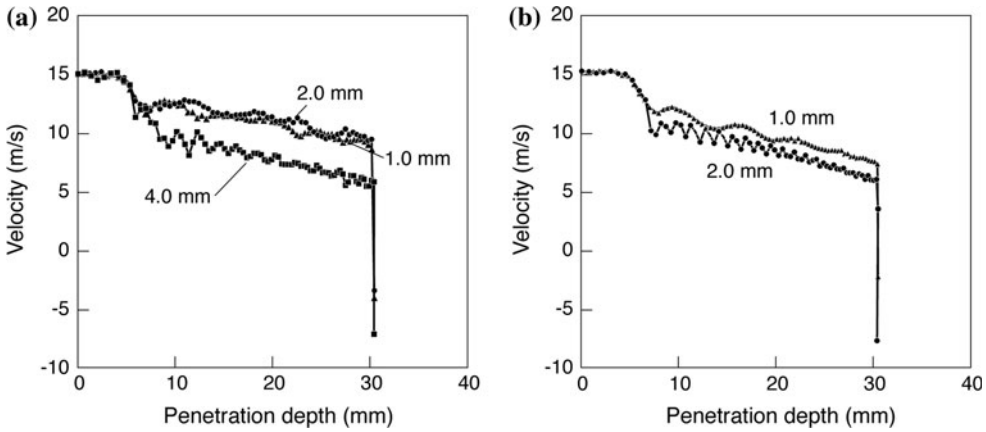

Fig. 8 The effect of cortical bone thickness is examined by holding the dart diameter at a constant 3.0 mm. The Bone 1 constitutive model was used. Results for a magnesium dart (**a**) and a PLA dart (**b**) are included. Curves corresponding to complete failures were not included

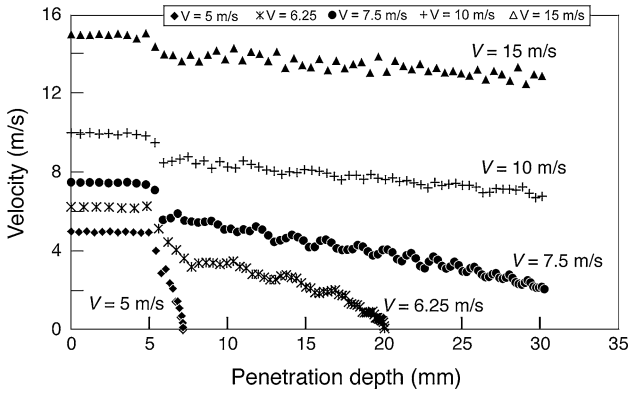

Fig. 9 The velocity-depth profiles for a 1.5 mm magnesium dart penetrating a 2.0 mm cortical bone (Bone 1) layer at varying initial velocities. The mass of the needle is held constant so the initial kinetic energy varies with the initial velocity

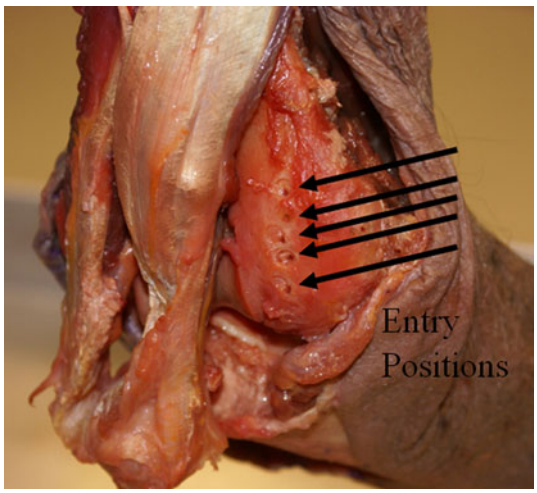

Fig. 10 Distal view of the humeral epiphysis. The entry locations of five 1.5 mm diameter PLA darts are visible

pins generally penetrated very well for all diameters except for the 1.5 mm diameter with a 4.0 mm cortical wall, in which high contact stresses caused excessive plastic deformation of the dart tip. On the other hand, PLA often performed poorly and a 1.5 mm diameter is not suitable for most fracture fixation applications. In fact, the PLA is suitable only for thin cortical walls (1.0 mm) according to the current model. These observations, however, do not account for elastic recovery of the bone. It is possible that the bone could recover and compress the darts resulting in good fixation even in the cases identified as having significant tip deformation (Groups C and D).

In most cases, the bone model (Bone 1 vs. Bone 2) had little effect on dart penetration or deformation (Table 2). The only effect for both magnesium and PLA was for the smallest dart diameter (1.5 mm). Not surprisingly, the Bone 2 model adversely affected penetration for the small darts but only in limited fashion. This is consistent with the notion that both Bone 1 and 2 are models suggested for the same material so it is expected that results should be relatively insensitive to material model selected. Over the ranges tested, it was shown that dart diameter has a more significant effect than cortical bone thickness (e.g. Figs. 7, 8). This was expected since the amount of deformed and fractured bone increases linearly with cortical thickness but increases with the square of the dart diameter. This is true since all the elements beneath the dart tip experience full material failure in the current model.

From the parametric study concerning initial velocity, it was observed that the darts to not penetrate appreciably beyond the needle stroke due to their low momentum regardless of insertion speed. Thus, for reasonably high speeds, such as those that can be obtained in a pneumatic or electric powered nailer, higher speeds/kinetic energies are preferable to ensure full penetration. The magnesium darts successfully survived dynamic insertion for all velocity and kinetic energy levels inspected for the 1.5 mm diameter dart and 2.0 mm cortical bone.

It is acknowledged that the assumptions of isotropy and von Mises plasticity are not realistic for bone despite their prevalence in many FEA studies [44]. However these

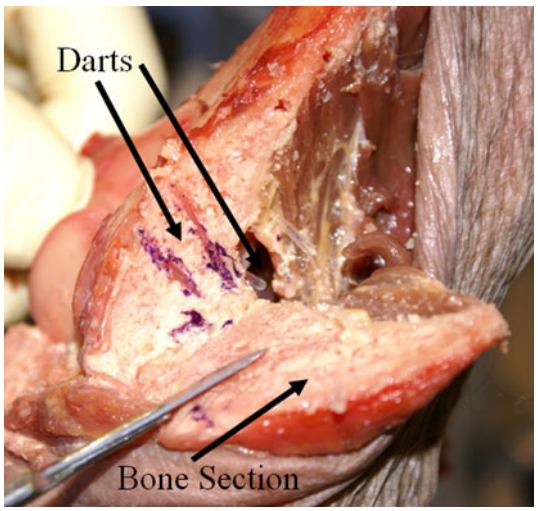

Fig. 11 Another view of the distal humeral epiphysis. A section of the bone was removed to expose the inserted darts. Two darts were exposed (highlighted with a *surgical pen*). Two other dart tips can be seen protruding from the second cortical wall. Note the thin cortical layer, estimated to be less than 1 mm in thickness

assumptions were necessary to achieve a full material description at high strain rates. Compressive and/or shear properties were applied if available since most of the relevant deformations were expected to be compressive or shear-like in nature.

One potential limitation of the model was the use of the element deletion scheme. The element deletion approach was necessary since both the cortical and cancellous bone were modeled with continuum elements. If a cohesive element model was used for the current geometry, there would be nowhere for fracture debris to flow which would prevent penetration. This does not reflect the fact that cancellous bone is a highly porous material, with porosities ranging from 50–95% [44]. As the dart penetrates, any cortical and cancellous debris would likely be pushed into the surrounding pore space where it would have minimal effects on penetration resistance. Since only approximate results were expected in the current model, the failed elements were deleted from mesh, thereby neglecting the volume of the fracture debris. It should be noted, however, that element deletion is a popular strategy for impact simulations using the finite element method [45–47].

The model was solved using ABAQUS/Explicit. This explicit solution method is recommended for very high speed, discontinuous events with large displacements and complex contact interactions which are all characteristic of the current penetration model. The explicit solution method uses a central difference operator to step the solution through time and is only conditionally stable. To ensure stability of the solution, ABAQUS internally calculates the step size based on element size and wave speed through

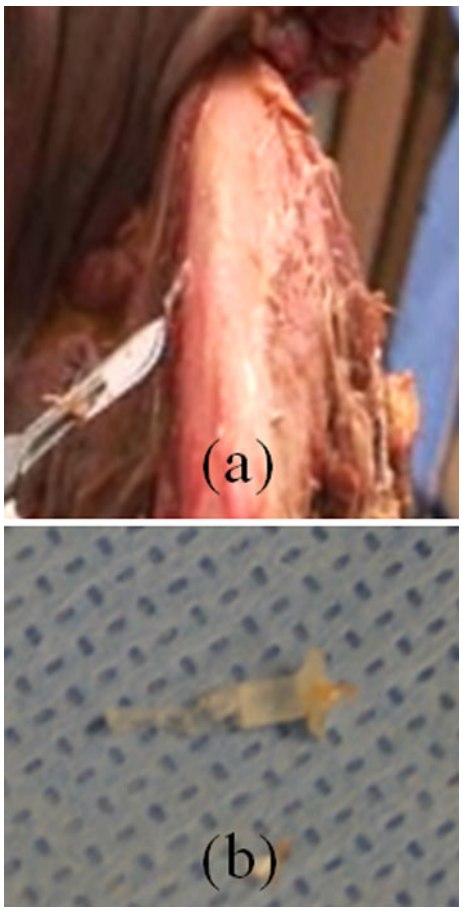

Fig. 12 **a** The scalpel points to a dart that failed to penetrate the humeral shaft. Only the tip embedded and the remainder of the dart hangs from the surface. **b** A portion of a dart that jammed inside the nozzle of the gun and was pulled free. Note the severely mushroomed tip

each material. Time steps are necessarily small, but each step is computationally inexpensive. For example the initial time step was on the order of 10^{-8} s for a 4.0 ms penetration event. To ensure validity of the solution, ABAQUS also checks for extreme deformation speeds in the elements which can be a sign of unrealistic deformations [24].

4.2 Model and experimental comparisons

The cadaveric bone results support the validity of the model. In both cases, the darts embedded flush with the bone surface after needle disengagement. Referring to Table 2, the model predicted that a 1.5 mm diameter PLA dart was capable of achieving full penetration in bone but would suffer moderate tip deformation (Group C). In the cadaveric bone, the PLA darts were capable of penetrating a cortical shell that was slightly less than 1 mm thick with no tip deformation (Figs. 10, 11). In contrast, it can be

noted from Table 2 that the model predicted a 1.5 mm PLA dart to be incapable of penetrating a 2 or 4 mm cortical shell. Gross levels of deformation were seen. This agrees with the findings from the experimental work, namely that the darts were incapable of penetrating mid-shaft where the cortical shell was certainly greater than 2 mm thick (Fig. 12). Note that these comparisons were made using the Bone 1 model which is the weaker of the two cortical bone constitutive models. This is appropriate since the cadaver bone was harvested from an elderly person, likely with inferior bone quality.

It is acknowledged that these comparisons do not stand as full quantitative validation of the model. Tests were only performed on a single bone specimen with unspecified mechanical properties. However, the model seems to capture an important qualitative trend, namely that there is some threshold value for cortical thickness above which 1.5 mm diameter PLA darts cannot penetrate. The exact value of the threshold thickness may not correlate exactly due to approximations in the model, but the fact the model captures the transitional behavior in penetration performance over a realistic range in cortical thickness is promising.

5 Conclusions

The results of the finite element simulations indicate that both magnesium and PLA have potential for use as high-speed fracture fixation darts. The finite element model predicts the following:

a) For magnesium darts successful penetration occurred in almost every circumstance regardless of the bone model used. The only exception was for the smallest diameter (1.5 mm) and thickest cortical shell where high contact stresses caused excessive deformation (4.0 mm).
b) PLA was acceptable for a number of circumstances but often encountered severe tip deformation and incomplete penetration.
c) For both magnesium and PLA the amount of tip deformation is reduced with increasing diameter. The PLA darts may only be suitable at a diameter of 4.0 mm or higher.
d) The behavior of the darts for all diameters, materials, and cortical bone dimensions was consistent regardless of the bone constitutive model used.
e) The study that varied velocity and kinetic energy suggests that a minimum threshold energy level is needed for complete penetration. It was also observed that the dart penetration is determined by the extent of needle travel. For this reason, the amount of kinetic energy used to dynamically insert a dart should be as high as is practical while maintaining this kinematic condition.

Experimental work with PLA darts and cadaver bone showed that 1.5 mm PLA darts are capable of penetrating thin cortical shells. However, with thicker cortical bone, the PLA saw high levels of tip deformation that prevented penetration. The experimental results show that the relevant subset of model results is predicting correct behavior.

Acknowledgments The authors would like to acknowledge the funding of Zimmer. The research was also supported by the U.S. Army Medical Research and Materiel Command, Contract W81XWH-09-1-0741. In addition the authors would like acknowledge the financial support of Professor Mark Jackson of AUT University, allowing for the collaboration between the University of Notre Dame and AUT University.

References

1. Farley GL. Repairing fractured bones by use of bioabsorbable composites (NASA Technical Brief LAR-16354-1). National Aeronautics and Space Administration, Langley Research Center. 2006.
2. Miller DL, Goswami T. A review of locking compression plate biomechanics and their advantages as internal fixators in fracture healing. Clin Biomech. 2007;22:1049–62.
3. Ezquerro F, Jiminez S, Perez A, Prado M, de Diego G, Simon A. The influence of wire positioning upon the initial stability of scaphoid fractures fixed using Kirschner wires: a finite element study. Med Eng Phys. 2007;29:652–60.
4. Gefen A. Optimizing the biomechanical compatibility of orthopaedic screws for bone fracture fixation. Med Eng Phys. 2002;24:337–47.
5. Duda GN, Kirchner H, Wilke HJ, Claes L. A method to determine the 3-D stiffness of fracture fixation devices and its application to predict inter-fragmentary movement. J Biomech. 1998;31:247–52.
6. Staiger MP, Pietak AM, Huadmai J, Dias G. Magnesium and its alloys as orthopedic biomaterials: a review. Biomater. 2006;27:1728–34.
7. Yamadi S, Kobayashi S. Effects of strain rate on the mechanical properties of tricalcium phosphate/poly(L-lactide) composites. J Mater Sci: Mater Med. 2009;20:67–74.
8. Gupta AP, Kumar V. New emerging trends in synthetic biodegradable polymers–polylactide: a critique. Eur Polym J. 2007;43:4053–74.
9. Sarasua JR, Arraiza AL. Crystallinity and mechanical properties of optically pure polylactides and their blends. Polym Eng Sci. 2005;45:745–53.
10. Claes LE, Ignatius AA, Rehm KE, Scholz C. New bioresorbable pin for the reduction of small bony fragments: design, mechanical properties and in vitro degradation. Biomater. 1996;17:1621–6.
11. Wen CE, Yamada Y, Shimojima K, Chino Y, Hosokawa H, Mabuchi M. Compressibility of porous magnesium foam: dependence on porosity and pore size. Mater Lett. 2004;58:357–60.
12. Denkena B, Lucas A. Biocompatible magnesium allows as absorbable implant materials–adjusted surface and subsurface properties by machining processes. Ann CIRP. 2007;56:113–6.
13. Mueller W, de Mele M, Nascimento M, Zeddies M. Degradation of magnesium and its alloys: dependence on the composition of

the synthetic biological media. J Biomed Mater Res. 2009;90A: 487–95.
14. Song WQ, Beggs P, Easton M. Compressive strain-rate sensitivity of magnesium-aluminum die casting alloys. Mater Des. 2009;30:642–8.
15. Witte F, Kaese V, Haferkamp H, Switzer E, Meyer-Lindenberg A, Wirth CJ, Windhagen H. In vivo corrosion of four magnesium alloys and the associated bone response. Biomater. 2005;26: 3557–63.
16. Xu L, Yu G, Zhang E, Pan F, Yang K. In vivo corrosion behavior of Mg–Mn–Zn alloy for bone implant application. J Biomed Mater Res. 2007;83A:703–11.
17. Witte F, Fischer J, Nellesen J, Crostack HA, Kaese V, Pisch A, Beckmann F, Windhagen H. In vitro and in vivo corrosion measurements of magnesium alloys. Biomater. 2006;27:1013–8.
18. Ferguson SJ, Weber U, von Rechenberg B, Mayer J. Enhancing the mechanical integrity of the implant-bone interface with BoneWelding® technology: determination of Quasi-Static interfacial strength and fatigue resistance. J Biomed Mater Res Part B. 2006;77B:13–20.
19. Kincaid B, Schroder L, Mason J. Measurement of orthopedic cortical bone screw insertion performance in cadaver bone and model materials. Exp Mech. 2007. doi:10.1007/s11340-007-9056-6.
20. Newman DL, Dougherty G, Al Obaid A, Al Hajrasy H. Limitations of clinical CT in assessing cortical thickness and density. Phys Med Biol. 1998;43:619–26.
21. Singh S. Ultrasonic non-destructive measurements of cortical bone thickness in human cadaver femur. Ultrason. 1989;27: 107–13.
22. Moilanen P, Talmant M, Bousson V, Nicholson PHF, Cheng S, Timonen J, Laugier P. Ultrasonically determined thickness of long cortical bones: two-dimensional simulations of in vitro experiments. J Acoust Soc Am. 2007;122(3):1818–26.
23. MacNeil JA, Boyd SK. Accuracy of high-resolution peripheral qualitative computed tomography for measurement of bone quality. Med Eng Phys. 2007;29:1096–105.
24. ABAQUS User's Manual. ABAQUS 6.8-EF2, SIMULIA, Dassault Systemes.
25. Li Z, Lambros J. Strain rate effects on the thermomechanical behavior of polymers. Int J Solids Struct. 2001;38:3549–62.
26. Hansen U, Zioupos P, Simpson R, Currey JD, Hynd D. The effect of strain rate on the mechanical properties of human cortical bone. J Biomech Eng. 2008. doi:10.1115/1.2838032.
27. McElhaney JH, Byars EF. Dynamic response of biological materials. In: Winter annual meeting of the American Society of Mechanical Engineers, ASME Human Factors Division. ASME. 1965.
28. Linde F, Norgaard P, Hvid I, Odgaard A, Soballe K. Mechanical properties of trabecular bone. dependency on strain rate. J Biomech. 1991;24(9):803–9.
29. Shim VPW, Yang LM, Lie JF, Lee VS. Characterisation of the dynamic compressive mechanical properties of cancellous bone from the human cervical spine. Int J Impact Eng. 2005;32: 525–40.
30. Ouyang J, Yang GT, Wu WZ, Zhu QA, Zhong SZ. Biomechanical characteristics of human trabecular bone. Clin Biomech. 1997;12:522–4.
31. Morgan EF, Keaveny TM. Dependence of yield strain of human trabecular bone on anatomic site. J Biomech. 2001;34:569–77.
32. Ford CM, Keaveny TM. The dependence of shear failure properties of trabecular bone on apparent density and trabecular orientation. J Biomech. 1996;29(10):1309–17.
33. Jepsen KJ, Davy DT. Comparison of damage accumulation measures in human cortical bone. J Biomech. 1997;30(9):891–4.
34. Mendelson A. Elastic-plastic torsion problem for strain-hardening materials (NASA Technical Note D-4391). National Aeronautics and Space Administration, Lewis Research Center. 1968.
35. Garnier KB, Dumas R, Rumelhart C, Arlot ME. Mechanical characterization in shear of human femoral cancellous bone: torsion and shear tests. Med Eng Phys. 1999;21:641–9.
36. Rincon-Kohli L, Zysset PK. Multi-axial mechanical properties of human trabecular bone. Biomech Model Mechanobiol. 2009;8: 195–208.
37. Kopperdahl DL, Keaveny TM. Yield strain behaviour of trabecular bone. J Biomech. 1998;31:601–8.
38. Norman TL, Nivargikar SV, Burr DB. Resistance to crack growth in human cortical bone is greater in shear than in tension. J Biomech. 1996;29:1023–31.
39. Feng Z, Rho J, Han S, Ziv I. Orientation and loading condition dependence of fracture toughness in cortical bone. Mater Sci Eng C. 2000;11:41–6.
40. Cook RB, Zioupos P. The fracture toughness of cancellous bone. J Biomech. 2009;42:2054–60.
41. Tomar V. Insights into the effects of tensile and compressive loadings on microstructure dependent fracture of trabecular bone. Eng Fract Mech. 2009;76:884–97.
42. Lim LT, Auras R, Rubino M. Processing technologies for poly(lactic acid). Prog Polym Sci. 2008;33:820–52.
43. Haibach R. Injection-molding degradation of biodegradable polylactide. Technical conference of the society of plastics engineers. ANTEC. 2007;4:2043–7.
44. Doblare M, Garcia JM, Gomez MJ. Modelling bone tissue fracture and healing: a review. Eng Fract Mech. 2004;71:1809–40.
45. Shin H, Lee HJ, Yoo YH, Lee W. A determination procedure for element elimination criterion in finite element analysis of high-strain-rate impact/penetration phenomena. JSME Int J Ser A. 2004;47(1):35–41.
46. Campbell J, Vignjevic R. Development of lagrangian hydrocode modelling for debris impact damage prediction. Int J Impact Eng. 1997;20:143–52.
47. Chen EP. Numerical simulation of penetration of aluminum targets by spherical-nose steel rods. Theor Appl Fract Mech. 1995; 22:159–64.
48. MatWeb Material Property Data: www.matweb.com. Accessed 1 Feb 2010.
49. Dong XN, Guo XE. The dependence of transversely isotropic elasticity of human femoral cortical bone on porosity. J Biomech. 2004;37:1281–7.